

# Molybdenum disulfide quantum dots decorated bismuth sulfide as a superior noble-metal-free photocatalyst for hydrogen evolution through harnessing a broad solar spectrum

## Citation for published version:

Lee, WPC, Kong, XY, Tan, LL, Gui, MM, Sumathi, S & Chai, S-P 2018, 'Molybdenum disulfide quantum dots decorated bismuth sulfide as a superior noble-metal-free photocatalyst for hydrogen evolution through harnessing a broad solar spectrum', *Applied Catalysis B: Environmental*.  
<https://doi.org/10.1016/j.apcatb.2018.03.019>

## Digital Object Identifier (DOI):

[10.1016/j.apcatb.2018.03.019](https://doi.org/10.1016/j.apcatb.2018.03.019)

## Link:

[Link to publication record in Heriot-Watt Research Portal](#)

## Document Version:

Peer reviewed version

## Published In:

Applied Catalysis B: Environmental

## Publisher Rights Statement:

© 2018 Elsevier B.V.

## General rights

Copyright for the publications made accessible via Heriot-Watt Research Portal is retained by the author(s) and / or other copyright owners and it is a condition of accessing these publications that users recognise and abide by the legal requirements associated with these rights.

## Take down policy

Heriot-Watt University has made every reasonable effort to ensure that the content in Heriot-Watt Research Portal complies with UK legislation. If you believe that the public display of this file breaches copyright please contact [open.access@hw.ac.uk](mailto:open.access@hw.ac.uk) providing details, and we will remove access to the work immediately and investigate your claim.

## Accepted Manuscript

Title: Molybdenum disulfide quantum dots decorated bismuth sulfide as a superior noble-metal-free photocatalyst for hydrogen evolution through harnessing a broad solar spectrum

Authors: W.P. Cathie Lee, Xin Ying Kong, Lling-Lling Tan, Meei Mei Gui, S. Sumathi, Siang-Piao Chai



PII: S0926-3373(18)30209-1  
DOI: <https://doi.org/10.1016/j.apcatb.2018.03.019>  
Reference: APCATB 16477

To appear in: *Applied Catalysis B: Environmental*

Received date: 27-12-2017  
Revised date: 15-2-2018  
Accepted date: 5-3-2018

Please cite this article as: Lee WPC, Kong XY, Tan L-L, Gui MM, Sumathi S, Chai S-P, Molybdenum disulfide quantum dots decorated bismuth sulfide as a superior noble-metal-free photocatalyst for hydrogen evolution through harnessing a broad solar spectrum, *Applied Catalysis B, Environmental* (2018), <https://doi.org/10.1016/j.apcatb.2018.03.019>

This is a PDF file of an unedited manuscript that has been accepted for publication. As a service to our customers we are providing this early version of the manuscript. The manuscript will undergo copyediting, typesetting, and review of the resulting proof before it is published in its final form. Please note that during the production process errors may be discovered which could affect the content, and all legal disclaimers that apply to the journal pertain.

# Molybdenum Disulfide Quantum Dots Decorated Bismuth Sulfide as a Superior Noble-Metal-Free Photocatalyst for Hydrogen Evolution through Harnessing a Broad Solar Spectrum

W. P. Cathie Lee,<sup>[a]</sup> Xin Ying Kong,<sup>[a]</sup> Lling-Lling Tan,<sup>[b]</sup> Meei Mei Gui,<sup>[c]</sup> S. Sumathi,<sup>[d]</sup> and Siang-Piao Chai<sup>\*[a]</sup>

<sup>[a]</sup> Multidisciplinary Platform of Advanced Engineering, Monash University, Jalan Lagoon Selatan, 47500 Bandar Sunway, Selangor, Malaysia

<sup>[b]</sup> School of Engineering and Physical Sciences, Heriot-Watt University Malaysia, Jalan Venna P5/2, Precinct 5, 62200 Putrajaya, Malaysia

<sup>[c]</sup> Nanotechnology and Integrated Bioengineering Centre, University of Ulster, Belfast, BT37 OQB Northern Ireland

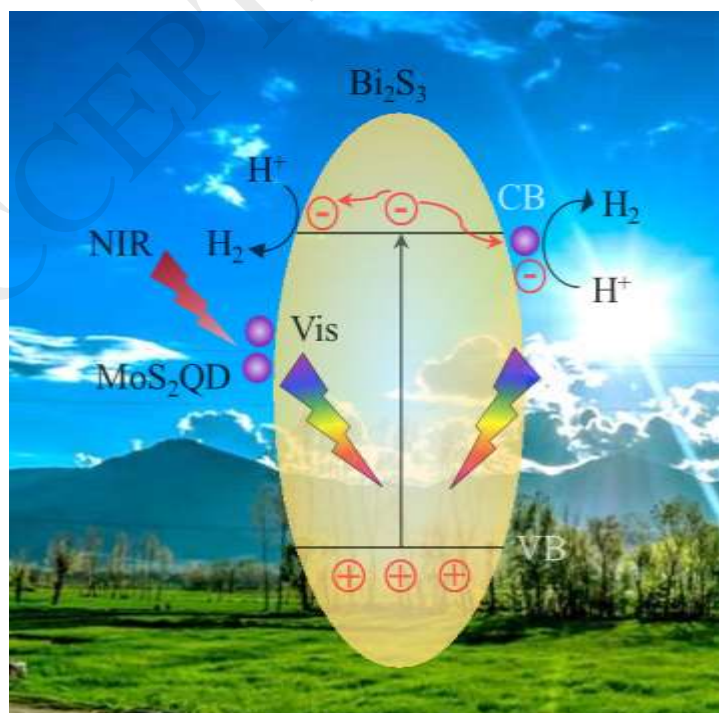
<sup>[d]</sup> Faculty of Engineering and Green Technology, Universiti Tunku Abdul Rahman, Kampar Campus, Jalan Universiti, Bandar Barat, 31900 Kampar, Perak, Malaysia

\*Corresponding author:

Tel: +603-55146234; Fax: +603-55146207

E-mail address: chai.siang.piao@monash.edu

## GRAPHICAL ABSTRACT



## Highlights

- Photoactivity of MoS<sub>2</sub>QDs doped Bi<sub>2</sub>S<sub>3</sub> extended from visible to NIR range
- Bi-functional roles of MoS<sub>2</sub>QDs as electron entrapment sites and spectral converters
- The highest H<sub>2</sub> evolution of 17.7 mmol/h.g was achieved under stimulated solar light

## Abstract

Molybdenum disulfide quantum dots (MoS<sub>2</sub>QDs) decorated bismuth sulfide (Bi<sub>2</sub>S<sub>3</sub>) photocatalyst was synthesized. Photoluminescence characterization showed that the as-developed MoS<sub>2</sub>QDs possessed intriguing up-conversion and down-conversion properties, indicating their capability to harness energy from the light spectrum ranging from ultraviolet (UV) to near-infrared (NIR). In this study, the highest hydrogen yield of 17.7 mmol/h.g was achieved by 0.14MoS<sub>2</sub>QD/Bi<sub>2</sub>S<sub>3</sub>, which was almost 4.5 folds higher than that of undoped Bi<sub>2</sub>S<sub>3</sub> under stimulated solar light irradiation. Furthermore, examination of the 0.14MoS<sub>2</sub>QD/Bi<sub>2</sub>S<sub>3</sub> photocatalysts under NIR irradiation showed a significant photocurrent response and an accumulative H<sub>2</sub> yield of 53.6  $\mu$ mol/g after 6 h reaction. This is a major breakthrough as most photocatalysts can only be activated under UV and/or visible light irradiation. This work provides new insights into the design of MoS<sub>2</sub>QD/Bi<sub>2</sub>S<sub>3</sub> for harnessing energy from a broad solar spectrum to photocatalytically split water to produce hydrogen.

## 1.0 Introduction

Energy generation by fossil fuel combustion dominates the emission of carbon dioxide (CO<sub>2</sub>), the major contributor to climate change and global warming. The rapid industrialization and technological progress that permeates every facet of life have further escalated the rate of fossil fuel depletion and CO<sub>2</sub> emission. Therefore, an alternative fuel source that is both clean and renewable is of paramount importance. Hydrogen (H<sub>2</sub>), in particular is a promising candidate to replace fossil fuels owing to its high fuel value of ~143 kJ/g. Furthermore, the combustion of H<sub>2</sub> produces only water as by-product, rendering the process environmentally benign [1].

There are a variety of methods to produce H<sub>2</sub>, such as solar energy pyrogenic decomposition, photo-electrochemistry method, photocatalysis and solar energy combined with electrolytic process. Among these routes, the photocatalytic splitting of water to generate H<sub>2</sub> has been widely regarded as one of the most sustainable approaches as the process can be carried out under room temperature and atmospheric pressure, in the presence of light irradiation [2-6]. The redox reaction is initiated by photoexcitation when the energy of photons from the light source is equal to or greater than the band gap of a semiconductor photocatalyst. The electrons are then excited from the valence band (VB) to the conduction band (CB), where these electrons are subsequently consumed to produce H<sub>2</sub>. It is therefore crucial to develop an efficient photocatalyst which exhibits suitable redox potentials, broad light absorption, and high photostability throughout the reaction. Noble metals, such as Pt, Pd, Au and Ag, have been studied extensively to achieve high photocatalytic activity for H<sub>2</sub> production [7-11]. However, the scarcity of these precious metals and high production costs limit the practicality of using noble metals for photocatalytic H<sub>2</sub> production. Under such circumstances, it is essential to design and develop an efficient and noble-metal-free photocatalytic system.

In view of solar energy utilization, the search for semiconductor photocatalysts that can harvest the wide spectrum of solar light, from ultraviolet (UV) to near-infrared (NIR) wavelength, and simultaneously achieve efficient solar energy conversion remains as one of the most challenging missions. At present, most photocatalysts developed in literature are active in the UV and/or visible light region, while activity under NIR light still remains rare. Utilization of light from NIR region can be achieved by converting longer wavelength NIR light to shorter wavelength visible light by means of doping with rare earth materials [12, 13]. In addition, surface plasmonic effect possessed by noble metals has also been reported as an NIR harvester for photocatalysis [14, 15].

Owing to its unique properties and versatility for numerous applications, molybdenum disulfide (MoS<sub>2</sub>), has been gaining tremendous attention from researchers worldwide [16-18]. The crystal structure of MoS<sub>2</sub> consists of sandwiched layers S-Mo-S bonded through covalent bonds and each layer is held together by relatively weak van der

Waals forces. MoS<sub>2</sub> with bulk structure has an indirect band gap of *ca.* 1.0 eV, while its direct band gap energy is approximately 1.8 – 2.0 eV. With this sandwiched structure, MoS<sub>2</sub> comprises of unsaturated Mo and S edges that serve as active sites where they can bond with reactant molecules to initiate surface reactions. However, the limited active sites on the basal plane of MoS<sub>2</sub> have hindered the catalytic efficiency of MoS<sub>2</sub> [19]. Therefore, morphology engineering of MoS<sub>2</sub>, such as reducing the number of layers and sizes, has been widely studied in an effort to increase its catalytic activity through edge exposing [19]. By decreasing the layers of MoS<sub>2</sub>, the band gap of MoS<sub>2</sub> could be transformed from indirect band gap (~1.0 eV) to direct band gap (1.8 – 2 eV) [20, 21].

Among the different shapes and sizes of MoS<sub>2</sub>, zero-dimensional (0D) MoS<sub>2</sub> quantum dots (MoS<sub>2</sub>QDs) possess unique optical and electronic properties, which are vital in many applications, particularly photocatalysis [1, 22-25]. The quantum size of MoS<sub>2</sub>QDs not only results in an increase in unsaturated bonds, but higher exposed edges per surface area as well. The latter will in turn enable more hydrogen atoms to be bonded to the photocatalyst, thereby increasing the photocatalytic activity for H<sub>2</sub> generation. Furthermore, MoS<sub>2</sub>QDs have been reported to exhibit up-conversion properties [26, 27].

In our previous study, MoS<sub>2</sub> sheets were grown onto Bi<sub>2</sub>S<sub>3</sub> giving a core-shell like structure that was shown to be an efficient photocatalyst for H<sub>2</sub> production [28]. In this study, we further enhanced the performance of Bi<sub>2</sub>S<sub>3</sub>-based photocatalyst in water splitting with MoS<sub>2</sub>QDs under broad solar spectrum. To the best of our knowledge, this is the first time MoS<sub>2</sub>QDs has been reported to exhibit photoactivity under NIR light irradiation. The synthesis of MoS<sub>2</sub>QDs was carried out via a top-down approach with the aid of sonication. The unique and fascinating excitation-dependent photoluminescence emission of MoS<sub>2</sub>QDs was also thoroughly examined in this work. The photocatalytic enhancement of MoS<sub>2</sub>QD/Bi<sub>2</sub>S<sub>3</sub> catalyst revealed the significance of MoS<sub>2</sub> structure in achieving a higher efficiency for H<sub>2</sub> production.

## 2.0 Materials and Methods

### 2.1 Materials

Bismuth (III) nitrate pentahydrate (Bi(NO<sub>3</sub>)<sub>3</sub>·5H<sub>2</sub>O), thioacetamide (C<sub>2</sub>H<sub>5</sub>NS), N,N-dimethylformamide (DMF), sodium sulfide (Na<sub>2</sub>S) and sodium sulfite (Na<sub>2</sub>SO<sub>3</sub>) were supplied by Sigma Aldrich. Sodium tungstate dihydrate (Na<sub>2</sub>WO<sub>4</sub>·5H<sub>2</sub>O) and ethanol were supplied from Merck and Friendemann Schmidt Chemical, respectively. All the chemicals were of analytical reagent grade and were used as received without further purification. Deionized (DI) water with conductivity of 18.2 MΩ cm was used in all experiments.

## 2.2 MoS<sub>2</sub> quantum dots synthesis

MoS<sub>2</sub> quantum dots (MoS<sub>2</sub>QDs) were prepared through a sonochemical method following the procedure reported elsewhere [16] with modifications. In brief, bulk MoS<sub>2</sub> was first dispersed in 100 mL of DMF solution. Next, the MoS<sub>2</sub> suspended solution was placed in an ice-bath and underwent sonication at 300 W for 3 h. The sonicated solution was then left undisturbed overnight to allow the bulk MoS<sub>2</sub> to settle. The top 2/3 of the suspended solution was then extracted to a round bottom flask and heated under reflux to 140 °C for 6 h under constant stirring. The cooled suspension was then centrifuged for 10 minutes at 5000 rpm to allow the sediment and supernatant to separate. The supernatant was then centrifuged again at 14000 rpm for 15 minutes to obtain MoS<sub>2</sub> suspension. The supernatant was collected and dried in a vacuum oven and re-dispersed in DMF to obtain 8 mg/mL MoS<sub>2</sub>QDs suspension with concentration of 8 mg/mL.

## 2.3 Synthesis of MoS<sub>2</sub>QD/Bi<sub>2</sub>S<sub>3</sub> photocatalyst

Prior to obtaining MoS<sub>2</sub>QD/Bi<sub>2</sub>S<sub>3</sub>, Bi<sub>2</sub>WO<sub>6</sub> was first synthesized by dissolving 0.4 mmol of Na<sub>2</sub>WO<sub>4</sub>·5H<sub>2</sub>O and 0.8 mmol of Bi(NO<sub>3</sub>)<sub>3</sub>·5H<sub>2</sub>O in 100 mL of DI water under constant stirring for 1 h. The solution was subsequently heated in a Teflon-lined autoclave for 15 h at 160 °C. The precipitate was washed with DI water and ethanol before drying in an oven. The as-synthesized Bi<sub>2</sub>WO<sub>6</sub> was then suspended in DI water through sonication for 1 h. Thioacetamide was subsequently added to the suspended solution under constant mixing before adding a pre-calculated amount of MoS<sub>2</sub>QDs suspension. The solution was then heated to 200 °C for 24 h in a Teflon-lined autoclave. After allowing the autoclave to cool down naturally, the precipitate was then washed with DI water and ethanol before drying in an oven. The as-prepared samples were denoted as xMoS<sub>2</sub>QD/Bi<sub>2</sub>S<sub>3</sub>, where x = 0.07, 0.14, 0.17, 0.21 and 0.36 wt% of MoS<sub>2</sub>QDs content.

## 2.4 Material characterization

The structural properties of the samples were analyzed by powder X-ray diffraction (XRD) with Bruker D8 Discover X-ray diffractometer with CuK $\alpha$  radiation ( $\lambda$  = 0.15406 nm) at a scan rate of 0.02 s<sup>-1</sup>. Field-emission scanning electron microscope (FE-SEM, Hitachi SU8010) was used to study the surface morphology of the as-prepared samples. Transmission electron microscopy (TEM) and high resolution TEM (HR-TEM) images were attained with TECNAI G2 F20 microscope equipped with energy dispersive X-ray (EDX) at an accelerating voltage of 200 kV. The as-prepared samples were suspended in ethanol with the aid of sonication and dropped onto a carbon coated copper grid and dried at room temperature. The elemental content of the as-prepared samples, was measured using inductively coupled plasma-mass spectrometry (ICP-MS) (Agilent 7900 ICP-MS). X-ray photoelectron spectroscopy (XPS) analysis was carried out with X-ray microprobe PHI Quantera (Ulvac-PHI, INC.) equipped with monochromatic Al-K $\alpha$  ( $h\nu$  = 1486.6 eV) X-ray source. The optical properties of the as-synthesized photocatalyst were analyzed with diffuse

reflectance absorption spectra and ultraviolet-visible spectra using Agilent Cary 100. Photoluminescence (PL) measurements were performed using LS 55 PerkinElmer fluorescence spectrophotometer with an excitation wavelength of 320 nm.

## 2.5 Photoelectrochemical measurements

A three electrode electrochemical quartz cell consisting a working electrode, Pt counter electrode and Ag/AgCl saturated with 3 M KCl as reference electrode was used to measure transient photocurrent responses and electrochemical impedance spectroscopy (EIS) Nyquist plots. 0.5 M Na<sub>2</sub>SO<sub>4</sub> was used as an electrolyte for all the photoelectrochemical measurements. The working electrodes were prepared by suspending the samples in ethanol (1 mg/mL). The suspension solution was then drop-casted onto a fluorine-doped tin oxide (FTO) with an electroactive area of 1 cm<sup>2</sup>. The amplitude and frequency of the AC potential were 0.01 V and 100 Hz, respectively.

## 2.6 Photocatalytic hydrogen production

The experiments for photocatalytic H<sub>2</sub> production were carried out in a black box fitted with a Pyrex reactor in a N<sub>2</sub> environment at room temperature and atmospheric pressure. 3 mg of the as-prepared photocatalyst was dispersed in 120 mL aqueous solution. 0.5 M Na<sub>2</sub>S and 0.5 M Na<sub>2</sub>SO<sub>3</sub> were used as scavenger. To ensure that the photocatalytic system was free from atmospheric air, the system was purged with N<sub>2</sub> gas for 30 minutes before the commencement of the photocatalytic reaction. The irradiation light source used in this study was a 500 W Xenon arc lamp (CHF-XM-500W) fixed with optical filter (AM1.5) to mimic solar light. The sampling port was connected to an online gas chromatography (Agilent 7890A, TCD, Ar gas carrier) to analyze the product gas at a time interval of 1 h.

## 3.0 Results and Discussion

### 3.1 Structural and chemical characterization

The crystallographic structures of the as-developed samples were studied using XRD, as shown in Figure 1(a). No broadening of peaks was observed for all samples, indicating their high crystallinity nature. The diffraction peaks shown in Figure 1(a) matched well with the orthorhombic phases of Bi<sub>2</sub>S<sub>3</sub> (JCPDS #012-0320), thus confirming the successful synthesis of Bi<sub>2</sub>S<sub>3</sub> through the in-situ anion exchange approach. The diffraction peaks of Bi<sub>2</sub>WO<sub>6</sub> were not detected across the entire prepared samples ( $2\theta = 55.8^\circ$ ). This further verified the successful conversion of Bi<sub>2</sub>WO<sub>6</sub> to Bi<sub>2</sub>S<sub>3</sub>. The reason behind the absence of MoS<sub>2</sub>QDs diffraction peaks could be attributed to the small loading of MoS<sub>2</sub> on the composite materials. The structure and morphology of the as-prepared MoS<sub>2</sub>QDs doped Bi<sub>2</sub>S<sub>3</sub> were examined using FE-SEM and TEM. Figure 1(b)-(d) shows the microscopy images of the 0.14MoS<sub>2</sub>QD/Bi<sub>2</sub>S<sub>3</sub> sample. The FE-SEM images of 0.07, 0.21 and 0.36MoS<sub>2</sub>QD/Bi<sub>2</sub>S<sub>3</sub> are shown in Figure S1. These images revealed that all samples



exhibited the discoid shape of  $\text{Bi}_2\text{S}_3$ , which were similar to our previous observations [29]. The average size of  $\text{MoS}_2\text{QD}/\text{Bi}_2\text{S}_3$  samples was determined from FE-SEM to be *ca.* 1  $\mu\text{m}$ . The TEM image presented in Figure 1(c) divulged that the  $0.14\text{MoS}_2\text{QD}/\text{Bi}_2\text{S}_3$  sample consisted of multiple rod-shaped structures which were stacked to form the distinct discoid shape of  $\text{Bi}_2\text{S}_3$ . The  $\text{MoS}_2\text{QDs}$  can be observed under the high resolution TEM (Figure 1(d)) as marked by arrows. The inset of Figure 1(d) revealed a lattice fringe of 0.27 nm, ascribed to the (100) plane of  $\text{MoS}_2$ . TEM elemental mapping of  $0.14\text{MoS}_2\text{QD}/\text{Bi}_2\text{S}_3$  shown in Figure S2 confirmed the presence of Bi, S and Mo. Furthermore, the actual  $\text{MoS}_2\text{QDs}$  content of the as-prepared samples was determined using ICP-MS and the results are presented in Table S1.

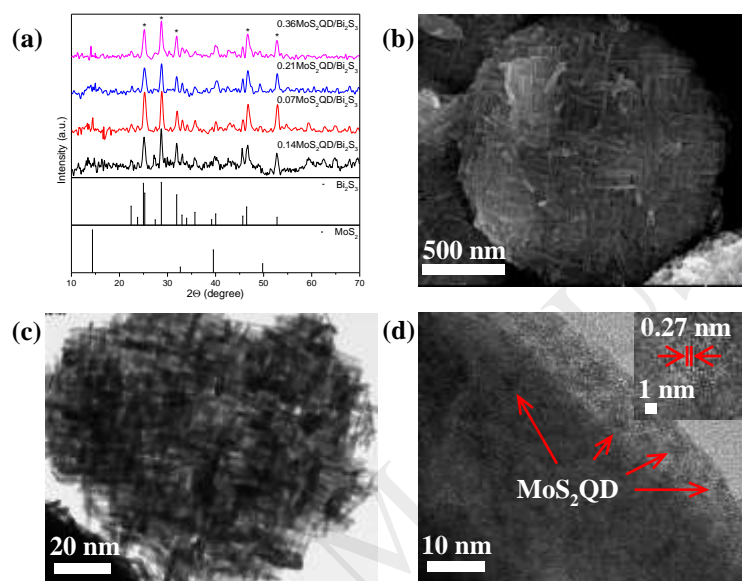


**Figure 1:** (a) XRD spectra of the  $\text{MoS}_2\text{QD}$ -doped  $\text{Bi}_2\text{S}_3$  samples synthesized with  $\text{Bi}_2\text{S}_3$  and  $\text{MoS}_2$  (b) FE-SEM, (c) TEM and (d) HR-TEM images of  $0.14\text{MoS}_2\text{QD}/\text{Bi}_2\text{S}_3$  (Inset: lattice spacing of  $\text{MoS}_2\text{QD}$  indicating (100) plane).

The surface valence state and surface chemical compositions of  $\text{MoS}_2\text{QDs}$  were further verified by X-ray photoelectron spectroscopy (XPS). The survey spectrum of  $\text{MoS}_2\text{QD}/\text{Bi}_2\text{S}_3$  is shown in Figure S3. All component elements Bi and Mo were identified in the wide scan, while no impurities were detected, indicating a high purity of the  $\text{MoS}_2\text{QD}/\text{Bi}_2\text{S}_3$  sample. The S element peak was not visible in the survey scan of  $0.14\text{MoS}_2\text{QD}/\text{Bi}_2\text{S}_3$ , as it could be shielded by the Bi element. This observation is in line with other reports published in literature [30, 31]. The high resolution orbit scan of individual elements is shown in Figure 2. The peaks detected at binding energies 228.9 and 232.5 eV (Figure 2(a)) can be ascribed to Mo  $3d_{5/2}$  and Mo  $3d_{3/2}$ , respectively. Both Mo peaks are typical for  $\text{Mo}^{4+}$  in  $\text{MoS}_2$  [32–34]. The peak at 225.7 eV can be assigned to S 2s. The peaks for Bi at 158.5 and 164.7 eV shown in Figure 2(b) correspond to Bi  $4f_{7/2}$  and Bi  $4f_{5/2}$  respectively. Following deconvolution, the peak at binding energy of 159.5 eV can be attributed to S  $2p_{3/2}$ . The presence of this peak confirms the existence of S element in the  $\text{MoS}_2/\text{Bi}_2\text{S}_3$  composite.

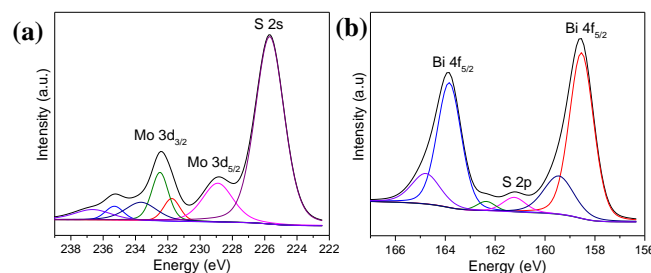


**Figure 2:** XPS spectra of 0.14MoS<sub>2</sub>QD/Bi<sub>2</sub>S<sub>3</sub> composite (a) Mo 3d and (b) Bi 4f and S 2p.

The optical properties of the as-synthesized samples were studied using UV-vis diffuse reflectance spectra (Figure S4). It is evident from Figure S4(a) that the light absorption ability of Bi<sub>2</sub>S<sub>3</sub> improved significantly upon doping with MoS<sub>2</sub>QDs instead of MoS<sub>2</sub> nanosheets. The light absorption ability of the samples was also observed to increase with the loading of MoS<sub>2</sub>QDs. It is also worth mentioning that the increase in light absorption was not limited to a specific wavelength, but was observable throughout the entire scanning spectrum i.e. 200 – 800 nm. This study clearly revealed the improved photoresponsiveness of the Bi<sub>2</sub>S<sub>3</sub> samples upon doping with MoS<sub>2</sub>QDs. The band gap energy of Bi<sub>2</sub>S<sub>3</sub> was also calculated by a modified Tauc plot approach (Figure S4(b)).

### 3.2 Photocatalytic H<sub>2</sub> production and mechanism of photocatalytic enhancement

The photocatalytic performance of the as-prepared samples were examined through the photocatalytic splitting of water under simulated solar light irradiation. The light spectrum is shown in Figure S5. Figure 3 shows the time-dependence H<sub>2</sub> yield (a) and the total product yield after 6 hours of reaction (b). The results obtained revealed the importance of MoS<sub>2</sub>QDs in improving the photocatalytic production of H<sub>2</sub>. As shown in Figure 3(b), pristine Bi<sub>2</sub>S<sub>3</sub> produced a total H<sub>2</sub> yield of 3.9 mmol/g.h after 6 h of light irradiation. Upon doping with 0.07 wt% MoS<sub>2</sub>QDs, the composite showed a H<sub>2</sub> production of 13.3 mmol/g.h, which was 3.4 times higher. The highest H<sub>2</sub> yield of 17.7 mmol/g.h was obtained when 0.14 wt% of MoS<sub>2</sub>QD were incorporated onto Bi<sub>2</sub>S<sub>3</sub>. In addition to that, the quantum size of MoS<sub>2</sub> was also responsible for the increase in photocatalytic performance due to significantly enhanced charge separation [33]. As the exposed S atoms are active sites for H<sub>2</sub> production, size reduction from bulk to QDs greatly increased the S atom for H<sup>+</sup> absorption to form S-H bond, giving rise to the increase in H<sub>2</sub> production. Further increase in the loading of QDs was found to reduce the efficiency of the photocatalyst. At higher loading of QDs, a shielding effect could have occurred, leading to the blockage of incident light from reaching the Bi<sub>2</sub>S<sub>3</sub> surface. In addition to remarkable activity, high photostability is also an essential characteristic that must be possessed by a good photocatalyst. To investigate the photostability of 0.14MoS<sub>2</sub>QD/Bi<sub>2</sub>S<sub>3</sub>, its performance in the photocatalytic production of H<sub>2</sub> was evaluated for four consecutive runs under

identical experimental conditions. As shown in Figure 3(c) and (d), the photoactivity of 0.14MoS<sub>2</sub>QD/Bi<sub>2</sub>S<sub>3</sub> was maintained after four cycles with a total reaction time of 24 h. 0.14MoS<sub>2</sub>QD/Bi<sub>2</sub>S<sub>3</sub> was able to retain more than 90% of photoactivity after 4 consecutive reaction run, thus indicating its superior photostability.

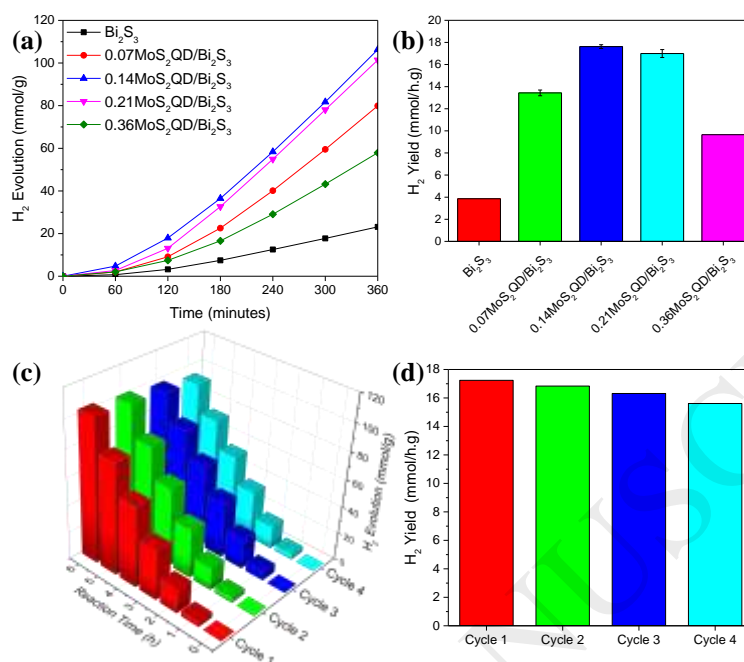


**Figure 3:** (a) Time course of photocatalytic H<sub>2</sub> evolution, (b) rate of photocatalytic H<sub>2</sub> production of all samples, (c) time course for 4 cycles of photocatalytic H<sub>2</sub> production over 0.14MoS<sub>2</sub>QD/Bi<sub>2</sub>S<sub>3</sub> and (d) rate of H<sub>2</sub> production for each cycles studied in 0.5 M Na<sub>2</sub>S/Na<sub>2</sub>SO<sub>3</sub> mixture under stimulated solar light irradiation for duration of 6 h.

To verify the activity of MoS<sub>2</sub>QD/Bi<sub>2</sub>S<sub>3</sub> photocatalyst under NIR light ( $\lambda > 700$  nm), 0.14MoS<sub>2</sub>QD/Bi<sub>2</sub>S<sub>3</sub> was subjected to photocatalytic H<sub>2</sub> production under similar reaction conditions, but under NIR light illumination instead. The results, as presented in Figure 4(a), showed that MoS<sub>2</sub>QDs were able to harness the NIR light for H<sub>2</sub> production through water splitting. In order to understand the significance of this result, PL characterization was carried out on MoS<sub>2</sub>QDs. Figure 4(b) and (c) show the PL emission spectra of the MoS<sub>2</sub>QDs under different excitation wavelength, which disclosed the as-synthesized MoS<sub>2</sub>QDs exhibited intriguing excitation-dependent PL emission properties. This suggests that MoS<sub>2</sub>QDs not only acted as spectral harvesters, they also played a pivotal role as excellent spectral converters. This phenomenon could be attributed to the homogeneity of the as-developed MoS<sub>2</sub>QDs, further confirming the successful synthesis of quantum-sized MoS<sub>2</sub> through the facile sonochemical approach. In addition to the down-converted PL property, MoS<sub>2</sub>QDs also possess fascinating up-converted PL behavior as shown in Figure 4(c). Upon excitation under NIR irradiation (700 – 780 nm), the PL emission spectra were found to be in the range of 455 to 488 nm. This suggested that the as-fabricated MoS<sub>2</sub>QDs could up-convert long-wavelength NIR light to short-wavelength visible light. This is

exceptionally desirable in photocatalysis as it manifests that NIR region could also be harvested, hence maximizing the utilization of the solar spectrum. Although MoS<sub>2</sub>QDs suspension appeared as light brown solution under visible light irradiation, the MoS<sub>2</sub>QDs emitted bright blue light under UV irradiation, as displayed in Figure 4 (b) insets. This observation revealed that the MoS<sub>2</sub>QDs possessed strong fluorescence emissions [35, 36]. The photoactivity of 0.14MoS<sub>2</sub>QD/Bi<sub>2</sub>S<sub>3</sub> was further verified with transient photocurrent responses carried out under NIR irradiation. The results obtained were presented in Figure 4(d). The photocatalyst decorated with MoS<sub>2</sub>QDs showed strong photocurrent response under NIR irradiation. As a comparison, similar characterization was carried out for pristine Bi<sub>2</sub>S<sub>3</sub> and MoS<sub>2</sub> nanosheets grown directly onto Bi<sub>2</sub>S<sub>3</sub> (23MoS<sub>2</sub>NS/Bi<sub>2</sub>S<sub>3</sub>). As shown in Figure 4(d), the photocurrent response of pristine Bi<sub>2</sub>S<sub>3</sub> and 23MoS<sub>2</sub>NS/Bi<sub>2</sub>S<sub>3</sub> were significantly lower than that for 0.14MoS<sub>2</sub>QD/Bi<sub>2</sub>S<sub>3</sub>. This observation clearly indicates the superiority of MoS<sub>2</sub>QDs under NIR irradiation. Refer to ESI and Figure S6 for the justifications of selection of 23MoS<sub>2</sub>NS/Bi<sub>2</sub>S<sub>3</sub> as a control sample. Further experiments were carried out to investigate the effects of MoS<sub>2</sub> structure on the photocatalytic activity. As presented in Figure S7, when bulk MoS<sub>2</sub> was used as photocatalyst for H<sub>2</sub> water splitting, a negligible amount of H<sub>2</sub> was produced. For 23MoS<sub>2</sub>NS/Bi<sub>2</sub>S<sub>3</sub>, 6.1 mmol/h.g of H<sub>2</sub> was yielded under similar experimental conditions. The enhancement in photoactivity was due to the intimate contact between MoS<sub>2</sub> and Bi<sub>2</sub>S<sub>3</sub>, which allowed rapid transfer and migration of photoinduced electrons and the subsequent suppression of electron-hole pair recombination [28]. When MoS<sub>2</sub>QDs were incorporated in place of MoS<sub>2</sub> nanosheets, the H<sub>2</sub> production increased to a whopping 17.7 mmol/h.g. The yield obtained was 4.5- and 2.9-folds higher than that of undoped Bi<sub>2</sub>S<sub>3</sub> and 23MoS<sub>2</sub>NS/Bi<sub>2</sub>S<sub>3</sub> respectively. This showed that only 0.14 wt% of MoS<sub>2</sub>QDs was required to produce H<sub>2</sub> yield with almost 3-fold higher than that of 23 wt% of MoS<sub>2</sub>NS used.

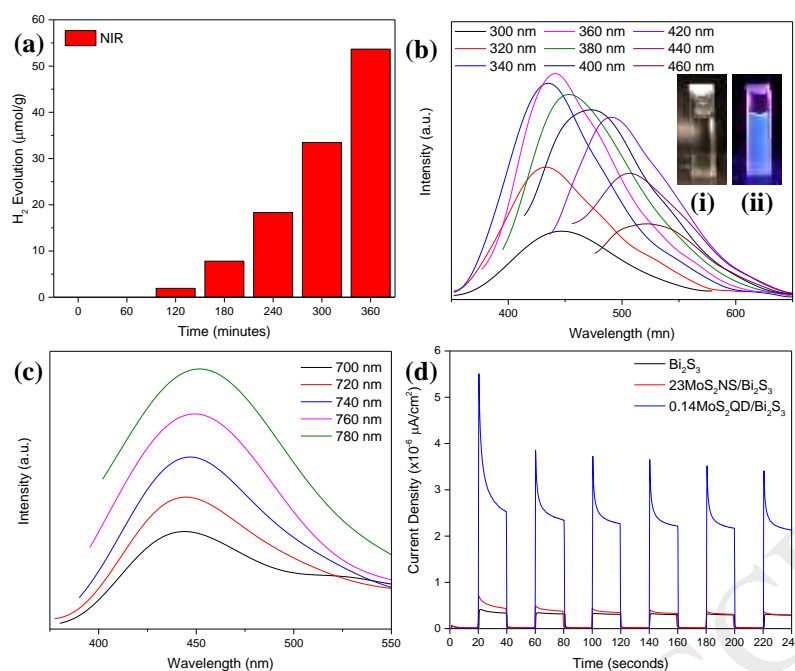


**Figure 4:** (a) H<sub>2</sub> evolution of 0.14MoS<sub>2</sub>QD/Bi<sub>2</sub>S<sub>3</sub> under NIR irradiation, (b) down-converted (Inset: MoS<sub>2</sub>QDs under (i) visible and (ii) UV light irradiation), (c) up-converted PL spectra of MoS<sub>2</sub>QDs, and (d) transient photocurrent response under NIR irradiation.

Electrochemical impedance spectroscopy (EIS) Nyquist plots of the samples are presented in Figure 5(a). The charge transfer resistance between the contact interface, working electrode and electrolyte was revealed by the arc radius from the Nyquist plot. The arc radius of 0.14MoS<sub>2</sub>QD/Bi<sub>2</sub>S<sub>3</sub> reduced significantly as compared to undoped Bi<sub>2</sub>S<sub>3</sub> and 23MoS<sub>2</sub>NS/Bi<sub>2</sub>S<sub>3</sub> (see Figure S8(a)). This implicates the importance of MoS<sub>2</sub>QDs on the photoactivity of Bi<sub>2</sub>S<sub>3</sub>. As the loading of MoS<sub>2</sub>QDs increased from 0.07 wt% to 0.14 wt%, the charge transfer resistance between the surface of the electrode and the electrolyte reduced. This observation implied a more efficient interfacial charge transfer within the composite. However, a further increase in MoS<sub>2</sub>QDs loading caused an increase in electron charge transfer resistance. Therefore, a balance between charge transfer mobility and electron hole recombination is desirable, and this was attained when 0.14wt% of MoS<sub>2</sub>QDs was doped onto Bi<sub>2</sub>S<sub>3</sub>.

To further verify the results, transient photocurrent responses were performed on the as-prepared samples (see Figure 5(b)). The current density was observed to have increased as soon as the light was switched on; photocurrent responses decreased to near zero when the light was turned off. In accordance to the photocatalytic experiments, 0.14MoS<sub>2</sub>QD/Bi<sub>2</sub>S<sub>3</sub> showed the highest photocurrent responses to the on/off light irradiation cycles as compared to the other loadings of MoS<sub>2</sub>QDs. This indicated that more electrons were able to migrate to the electrodes to produce a current flow. In addition, 0.14MoS<sub>2</sub>QD/Bi<sub>2</sub>S<sub>3</sub> showed superiority in transient photocurrent responses in comparison to undoped Bi<sub>2</sub>S<sub>3</sub> and 23MoS<sub>2</sub>NS/Bi<sub>2</sub>S<sub>3</sub> (Figure S8(b)), demonstrating efficient separation of photogenerated charges.

Photoluminescence (PL) analysis is shown in Figure 5(c). Suppression of the emission peak for 0.14MoS<sub>2</sub>QD/Bi<sub>2</sub>S<sub>3</sub> signified the delay in electron-hole pair recombination of the photocatalyst. As compared to 0.07, 0.21 and 0.36 wt% of MoS<sub>2</sub>QDs loading, the electron-hole recombination rate of 0.14MoS<sub>2</sub>QD/Bi<sub>2</sub>S<sub>3</sub> was the lowest, indicating that 0.14MoS<sub>2</sub>QD/Bi<sub>2</sub>S<sub>3</sub> was the most efficient composite for charge separation. This observation matches well with the H<sub>2</sub> production results reported earlier. Figure S8(c) shows the PL spectra for the as-synthesized MoS<sub>2</sub>QDs doped samples in this study. The spectra showed that 0.14MoS<sub>2</sub>QD/Bi<sub>2</sub>S<sub>3</sub> had the lowest peak intensity as compared to the other samples. This further demonstrated the significance of the MoS<sub>2</sub> structure, in which quantum dots were more efficient in suppressing electron-hole recombination, which in turn resulted in higher H<sub>2</sub> yield.

The schematic illustration of the photoexcited electron-hole pair separation for 0.14MoS<sub>2</sub>QD/Bi<sub>2</sub>S<sub>3</sub> is presented in Figure 5(d). Under light irradiation, electrons on Bi<sub>2</sub>S<sub>3</sub> were excited from the VB to the CB, which then reacted with adsorbed H<sup>+</sup> ions to form H<sub>2</sub> molecules. The enhancement of the photocatalytic production of H<sub>2</sub> can be attributed to the synergetic effect between MoS<sub>2</sub>QDs and Bi<sub>2</sub>S<sub>3</sub> where the photogenerated electrons on Bi<sub>2</sub>S<sub>3</sub> could transfer to MoS<sub>2</sub>QDs to take part in the H<sub>2</sub> production reaction. Furthermore, as a spectral converter, the MoS<sub>2</sub>QDs were capable of harnessing NIR light to drive the photocatalytic H<sub>2</sub> production. Through this, Bi<sub>2</sub>S<sub>3</sub> could utilize the up-converted light to excite electrons from the ground state for water reduction. Besides, the addition of MoS<sub>2</sub>QDs enhanced the visible light absorption and promoted charge transfer and separation, giving the photocatalyst a longer reaction lifetime.

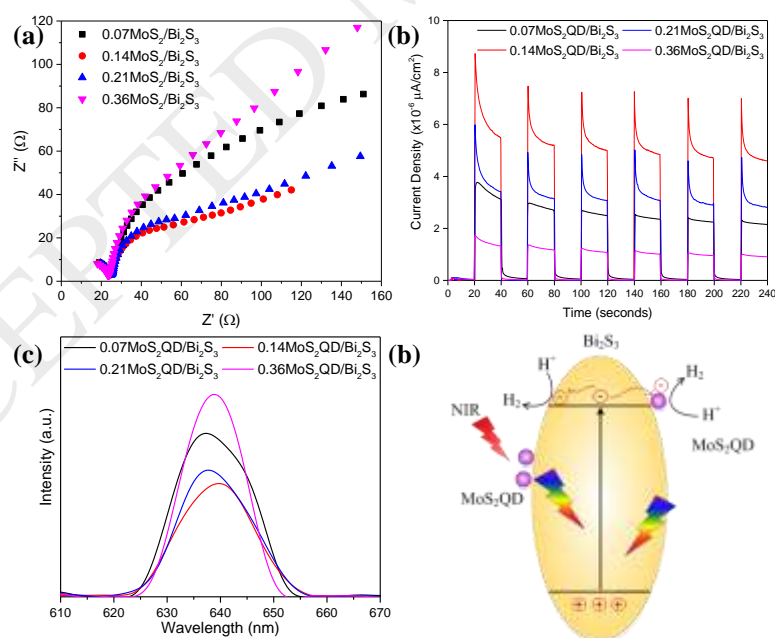


**Figure 5:** (a) EIS Nyquist plots, (b) transient photocurrent response under simulated solar light, (c) steady-state PL spectra of the as-prepared MoS<sub>2</sub>QDs doped samples and (d) schematic illustration of H<sub>2</sub> production under light irradiation.

#### 4.0 Conclusion

In summary, MoS<sub>2</sub>QDs decorated Bi<sub>2</sub>S<sub>3</sub> was successfully synthesized *via* a facile hydrothermal method. The presence of MoS<sub>2</sub>QDs has effectively enhanced the photocatalytic H<sub>2</sub> evolution for all samples. At an optimum loading of 0.14 wt% of MoS<sub>2</sub>QDs, the H<sub>2</sub> evolution rate was the highest at 17.7 mmol/h.g. The improvement was found to be 3.0- and 4.5-fold higher than that of control 23MoS<sub>2</sub>NS/Bi<sub>2</sub>S<sub>3</sub> and undoped Bi<sub>2</sub>S<sub>3</sub>, respectively. The enhancement is due to the synergistic effects between Bi<sub>2</sub>S<sub>3</sub> and MoS<sub>2</sub>QDs, in which the MoS<sub>2</sub>QDs played bi-functional roles as electron entrapment sites and spectral converters. This work demonstrated the importance of MoS<sub>2</sub>QDs and their potential in replacing noble metal co-catalysts for photocatalytic H<sub>2</sub> production under broad solar spectrum. MoS<sub>2</sub>QD/Bi<sub>2</sub>S<sub>3</sub> photocatalyst paves a new pathway for utilizing solar spectrum for H<sub>2</sub> production and a step closer to the realization of a fossil fuel-free world.

#### Acknowledgements

This work was financially supported by Monash University Malaysia under Advanced Engineering Platform and the Ministry of Higher Education (MOHE) Malaysia and Universiti Sains Malaysia (USM) under NanoMITE Long-term Research Grant Scheme (LRGS) (Ref no.: 203/PJKIMIA/6720009).

#### References

- [1] X. Jin, X. Fan, J. Tian, R. Cheng, M. Li, L. Zhang, MoS<sub>2</sub> quantum dot decorated g-C<sub>3</sub>N<sub>4</sub> composite photocatalyst with enhanced hydrogen evolution performance, *RSC Adv.*, 6 (2016) 52611-52619.
- [2] C. Ma, H. Zhu, J. Zhou, Z. Cui, T. Liu, Y. Wang, Y. Wang, Z. Zou, Confinement effect of monolayer MoS<sub>2</sub> quantum dots on conjugated polyimide and promotion of solar-driven photocatalytic hydrogen generation, *Dalton Transactions*, 46 (2017) 3877-3886.
- [3] F.A. Frame, F.E. Osterloh, CdSe-MoS<sub>2</sub>: A Quantum Size-Confined Photocatalyst for Hydrogen Evolution from Water under Visible Light, *J. Phys. Chem. C*, 114 (2010) 10628-10633.
- [4] B.-J. Ng, L.K. Putri, L.-L. Tan, P. Pasbakhsh, S.-P. Chai, All-solid-state Z-scheme photocatalyst with carbon nanotubes as an electron mediator for hydrogen evolution under simulated solar light, *Chem. Eng. J.*, 316 (2017) 41-49.
- [5] L.K. Putri, B.-J. Ng, W.-J. Ong, H.W. Lee, W.S. Chang, S.-P. Chai, Heteroatom Nitrogen- and Boron-Doping as a Facile Strategy to Improve Photocatalytic Activity of Standalone Reduced Graphene Oxide in Hydrogen Evolution, *ACS Appl. Mater. Interfaces*, 9 (2017) 4558-4569.
- [6] L.-L. Tan, W.-J. Ong, S.-P. Chai, A.R. Mohamed, Visible-light-activated oxygen-rich TiO<sub>2</sub> as next generation photocatalyst: Importance of annealing temperature on the photoactivity toward reduction of carbon dioxide, *Chem. Eng. J.*, 283 (2016) 1254-1263.
- [7] M.-Y. Xie, K.-Y. Su, X.-Y. Peng, R.-J. Wu, M. Chavali, W.-C. Chang, Hydrogen production by photocatalytic water-splitting on Pt-doped TiO<sub>2</sub>-ZnO under visible light, *Journal of the Taiwan Institute of Chemical Engineers*, 70 (2017) 161-167.



- [8] Z. Zhu, C.-T. Kao, B.-H. Tang, W.-C. Chang, R.-J. Wu, Efficient hydrogen production by photocatalytic water-splitting using Pt-doped TiO<sub>2</sub> hollow spheres under visible light, *Ceram. Int.*, 42 (2016) 6749-6754.
- [9] E.A. Kozlova, A.Y. Kurenkova, P.A. Kolinko, A.A. Saraev, E.Y. Gerasimov, D.V. Kozlov, Photocatalytic hydrogen production using Me/Cd<sub>0.3</sub>Zn<sub>0.7</sub>S (Me = Au, Pt, Pd) catalysts: Transformation of the metallic catalyst under the action of the reaction medium, *Kinet. Catal.*, 58 (2017) 431-440.
- [10] S.Y. Arzate Salgado, R.M. Ramírez Zamora, R. Zanella, J. Peral, S. Malato, M.I. Maldonado, Photocatalytic hydrogen production in a solar pilot plant using a Au/TiO<sub>2</sub> photo catalyst, *Int. J. Hydrogen Energy*, 41 (2016) 11933-11940.
- [11] J. Qin, J. Huo, P. Zhang, J. Zeng, T. Wang, H. Zeng, Improving the photocatalytic hydrogen production of Ag/g-C<sub>3</sub>N<sub>4</sub> nanocomposites by dye-sensitization under visible light irradiation, *Nanoscale*, 8 (2016) 2249-2259.
- [12] Y. Tang, W. Di, X. Zhai, R. Yang, W. Qin, NIR-Responsive Photocatalytic Activity and Mechanism of NaYF<sub>4</sub>:Yb,Tm@TiO<sub>2</sub> Core-Shell Nanoparticles, *ACS Catal.*, 3 (2013) 405-412.
- [13] M. Tou, Y. Mei, S. Bai, Z. Luo, Y. Zhang, Z. Li, Depositing CdS nanoclusters on carbon-modified NaYF<sub>4</sub>:Yb,Tm upconversion nanocrystals for NIR-light enhanced photocatalysis, *Nanoscale*, 8 (2016) 553-562.
- [14] M. Zhu, X. Cai, M. Fujitsuka, J. Zhang, T. Majima, Au/La<sub>2</sub>Ti<sub>2</sub>O<sub>7</sub> Nanostructures Sensitized with Black Phosphorus for Plasmon-Enhanced Photocatalytic Hydrogen Production in Visible and Near-Infrared Light, *Angew. Chem. Int. Ed.*, 56 (2017) 2064-2068.
- [15] Z. Zheng, T. Tachikawa, T. Majima, Single-Particle Study of Pt-Modified Au Nanorods for Plasmon-Enhanced Hydrogen Generation in Visible to Near-Infrared Region, *J. Am. Chem. Soc.*, 136 (2014) 6870-6873.
- [16] W. Xing, Y. Chen, X. Wang, L. Lv, X. Ouyang, Z. Ge, H. Huang, MoS<sub>2</sub> Quantum Dots with a Tunable Work Function for High-Performance Organic Solar Cells, *ACS Appl. Mater. Interfaces*, 8 (2016) 26916-26923.
- [17] J. Kibsgaard, Z. Chen, B.N. Reinecke, T.F. Jaramillo, Engineering the surface structure of MoS<sub>2</sub> to preferentially expose active edge sites for electrocatalysis, *Nat Mater*, 11 (2012) 963-969.
- [18] S. Wang, X. Li, Y. Chen, X. Cai, H. Yao, W. Gao, Y. Zheng, X. An, J. Shi, H. Chen, A Facile One-Pot Synthesis of a Two-Dimensional MoS<sub>2</sub>/Bi<sub>2</sub>S<sub>3</sub> Composite Theranostic Nanosystem for Multi-Modality Tumor Imaging and Therapy, *Adv. Mater.*, 27 (2015) 2775-2782.
- [19] Y. Li, L. Wang, T. Cai, S. Zhang, Y. Liu, Y. Song, X. Dong, L. Hu, Glucose-assisted synthesize 1D/2D nearly vertical CdS/MoS<sub>2</sub> heterostructures for efficient photocatalytic hydrogen evolution, *Chem. Eng. J.*, 321 (2017) 366-374.
- [20] T.P. Nguyen, W. Sohn, J.H. Oh, H.W. Jang, S.Y. Kim, Size-Dependent Properties of Two-Dimensional MoS<sub>2</sub> and WS<sub>2</sub>, *J. Phys. Chem. C*, 120 (2016) 10078-10085.
- [21] R. Ganatra, Q. Zhang, Few-Layer MoS<sub>2</sub>: A Promising Layered Semiconductor, *ACS Nano*, 8 (2014) 4074-4099.
- [22] X. Meng, Z. Li, H. Zeng, J. Chen, Z. Zhang, MoS<sub>2</sub> quantum dots-interspersed Bi<sub>2</sub>WO<sub>6</sub> heterostructures for visible light-induced detoxification and disinfection, *Appl. Catal. B.*, 210 (2017) 160-172.
- [23] D. Wang, Y. Xu, F. Sun, Q. Zhang, P. Wang, X. Wang, Enhanced photocatalytic activity of TiO<sub>2</sub> under sunlight by MoS<sub>2</sub> nanodots modification, *Appl. Surf. Sci.*, 377 (2016) 221-227.



- [24] X. Hao, Z. Jin, H. Yang, G. Lu, Y. Bi, Peculiar synergetic effect of MoS<sub>2</sub> quantum dots and graphene on Metal-Organic Frameworks for photocatalytic hydrogen evolution, *Appl. Catal. B.*, 210 (2017) 45-56.
- [25] X. Wang, S. Chen, M. Zhang, Y. Huang, S. Feng, D. Zhao, MoS<sub>2</sub> quantum dot-modified Ag/polyaniline composites with enhanced photogenerated carrier separation for highly efficient visible light photocatalytic H<sub>2</sub> evolution performance, *Catal. Sci. Tech.*, (2017).
- [26] H. Huang, C. Du, H. Shi, X. Feng, J. Li, Y. Tan, W. Song, Water-Soluble Monolayer Molybdenum Disulfide Quantum Dots with Upconversion Fluorescence, *Particle & Particle Systems Characterization*, 32 (2015) 72-79.
- [27] W. Gu, Y. Yan, C. Zhang, C. Ding, Y. Xian, One-Step Synthesis of Water-Soluble MoS<sub>2</sub> Quantum Dots via a Hydrothermal Method as a Fluorescent Probe for Hyaluronidase Detection, *ACS Appl. Mater. Interfaces*, 8 (2016) 11272-11279.
- [28] W.P.C. Lee, M.-M. Gui, L.-L. Tan, T.Y. Wu, S. Sumathi, S.-P. Chai, Bismuth sulphide-modified molybdenum disulphide as an efficient photocatalyst for hydrogen production under simulated solar light, *Catal. Commun.*, 98 (2017) 66-70.
- [29] W.P.C. Lee, F.-H. Wong, N.K. Attenborough, X.Y. Kong, L.-L. Tan, S. Sumathi, S.-P. Chai, Two-dimensional bismuth oxybromide coupled with molybdenum disulphide for enhanced dye degradation using low power energy-saving light bulb, *Journal of Environmental Management*, 197 (2017) 63-69.
- [30] N. Liang, J. Zai, M. Xu, Q. Zhu, X. Wei, X. Qian, Novel Bi<sub>2</sub>S<sub>3</sub>/Bi<sub>2</sub>O<sub>2</sub>CO<sub>3</sub> heterojunction photocatalysts with enhanced visible light responsive activity and wastewater treatment, *J. Mater. Chem. A*, 2 (2014) 4208-4216.
- [31] A. Rauf, M.S.A. Sher Shah, G.H. Choi, U.B. Humayoun, D.H. Yoon, J.W. Bae, J. Park, W.-J. Kim, P.J. Yoo, Facile Synthesis of Hierarchically Structured Bi<sub>2</sub>S<sub>3</sub>/Bi<sub>2</sub>WO<sub>6</sub> Photocatalysts for Highly Efficient Reduction of Cr(VI), *ACS Sustain. Chem. Eng.*, 3 (2015) 2847-2855.
- [32] B.A. Vanchura, P. He, V. Antochshuk, M. Jaroniec, A. Ferryman, D. Barbash, J.E. Fulghum, S.D. Huang, Direct Synthesis of Mesostructured Lamellar Molybdenum Disulfides Using a Molten Neutral n-Alkylamine as the Solvent and Template, *J. Am. Chem. Soc.*, 124 (2002) 12090-12091.
- [33] W. Gao, M. Wang, C. Ran, L. Li, Facile one-pot synthesis of MoS<sub>2</sub> quantum dots-graphene-TiO<sub>2</sub> composites for highly enhanced photocatalytic properties, *Chem. Commun.*, 51 (2015) 1709-1712.
- [34] F. Liu, Y. Jiang, J. Yang, M. Hao, Z. Tong, L. Jiang, Z. Wu, MoS<sub>2</sub> nanodot decorated In<sub>2</sub>S<sub>3</sub> nanoplates: a novel heterojunction with enhanced photoelectrochemical performance, *Chem. Commun.*, 52 (2016) 1867-1870.
- [35] S. Kumar, A.K. Ojha, B. Ahmed, A. Kumar, J. Das, A. Materny, Tunable (violet to green) emission by high-yield graphene quantum dots and exploiting its unique properties towards sun-light-driven photocatalysis and supercapacitor electrode materials, *Materials Today Communications*, 11 (2017) 76-86.
- [36] X.Y. Kong, W.L. Tan, B.-J. Ng, S.-P. Chai, A.R. Mohamed, Harnessing Vis-NIR broad spectrum for photocatalytic CO<sub>2</sub> reduction over carbon quantum dots-decorated ultrathin Bi<sub>2</sub>WO<sub>6</sub> nanosheets, *Nano Research*, 10 (2017) 1720-1731.